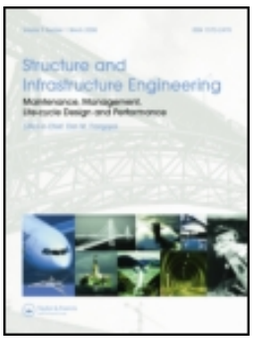

Taylor & Francis
Taylor & Francis Group

Structure and Infrastructure Engineering
Maintenance, Management, Life-Cycle Design and Performance

ISSN: 1573-2479 (Print) 1744-8980 (Online) Journal homepage: http://www.tandfonline.com/loi/nsie20

Automated image processing technique for detecting and analysing concrete surface cracks

Bang Yeon Lee , Yun Yong Kim , Seong-Tae Yi & Jin-Keun Kim

To cite this article: Bang Yeon Lee , Yun Yong Kim , Seong-Tae Yi & Jin-Keun Kim (2013) Automated image processing technique for detecting and analysing concrete surface cracks, Structure and Infrastructure Engineering, 9:6, 567-577, DOI: 10.1080/15732479.2011.593891

To link to this article: https://doi.org/10.1080/15732479.2011.593891

Published online: 30 Jun 2011.

Structure and Infrastructure Engineering
Vol. 9, No. 6, June 2013, 567–577

Taylor & Francis
Taylor & Francis Group

Automated image processing technique for detecting and analysing concrete surface cracks

Bang Yeon Lee[a], Yun Yong Kim[b]*, Seong-Tae Yi[c] and Jin-Keun Kim[d]

[a]*School of Architecture, Chonnam National University, Gwangju, Republic of Korea;* [b]*Department of Civil Engineering, Chungnam National University, Daejeon, Republic of Korea;* [c]*Department of Civil and Environmental Engineering, Inha Technical College, Incheon, Republic of Korea;* [d]*Department of Civil and Environmental Engineering, Korea Advanced Institute of Science and Technology, Daejeon, Republic of Korea*

(*Received 2 July 2008; final version received 29 May 2011; accepted 1 June 2011; published online 30 June 2011*)

In the present work, an image processing technique that automatically detects and analyses cracks in the digital image of concrete surfaces is proposed. The image processing technique automates the measurement of crack characteristics including the width, length, orientation and crack pattern. In the proposed technique, a morphological technique was applied to correct the non-uniform brightness of the background, and enhanced binarisation and shape analysis were used to improve the detection performance; furthermore, detailed algorithms to calculate the crack width, length, orientation and an artificial neural network to recognise crack patterns including horizontal, vertical, diagonal (-45°), diagonal ($+45^\circ$), and random cracks are proposed. An image processing program was developed for the proposed algorithm and a series of experimental and analytical investigations were performed to assess the validity of the algorithm. Then, the crack characteristics measured using the proposed technique were compared with those obtained using a conventional technique. The test results showed that the crack characteristics can be accurately measured and analysed using the proposed technique.

Keywords: concrete crack; crack detection; crack analysis; crack characteristics

1. Introduction

Cracks are a primary concern with the safety, durability, and serviceability of concrete structures and much effort has been made to minimise the negative effect of cracks. This study is based on measuring the crack characteristics such as the width, length, and orientation, and on establishing a database of such characteristics. However, much time and energy is required to obtain these measurements and to compile relevant data because it is generally undertaken manually. Therefore, many researchers have proposed several techniques based on an image processing, which enable faster and more efficient in measuring the cracks in concrete surfaces (Kaseko and Ritchie 1993, Ito *et al.* 2002, Schutter 2002, Sohn *et al.* 2005, Chen *et al.* 2006, Hutchinson and Chen 2006, Yamaguchi *et al.* 2008). In these methods, the crack detection detects cracks shown on an image of a concrete surface, and the crack analysis calculates the characteristics of the detected cracks, such as crack width, length and area. Recently, robot-based inspection systems equipped with machine vision have been proposed for bridges, tunnels and buried concrete pipes (Sinha and Fieguth 2006, Yu *et al.* 2007, Oh *et al.* 2009). However, crack-detection techniques have not been fully developed because the mathematical modelling of cracks has not yet been realised due to the random shapes of cracks. Furthermore, there is much noise in the image of concrete surface because concrete structures are exposed to the environment.

In the present work, the authors describe a new image processing technique that detects cracks and calculates the crack characteristics using images taken with a digital camera. The process of the proposed technique is similar to that developed in previous studies (Ito *et al.* 2002, Sohn *et al.* 2005, Chen *et al.* 2006, Hutchinson and Chen 2006, Sinha and Fieguth 2006, Yu *et al.* 2007, Yamaguchi *et al.* 2008, Oh *et al.* 2009) in terms of crack detection and analysis; however, this study focuses on improving the crack detection performance. A morphological technique is applied to correct the non-uniform brightness of the background, and an enhanced binarisation and shape analyses are also developed to improve the detection performance. Finally, detailed algorithms to calculate the crack width, length and orientation are proposed, and an artificial neural network is also developed to recognise the crack patterns.

2. Crack detection

The flow chart of the proposed algorithm is shown in Figure 1. The crack image taken with a digital

*Corresponding author. Email: yunkim@cnu.ac.kr

ISSN 1573-2479 print/ISSN 1744-8980 online

http://dx.doi.org/10.1080/15732479.2011.593891
http://www.tandfonline.com

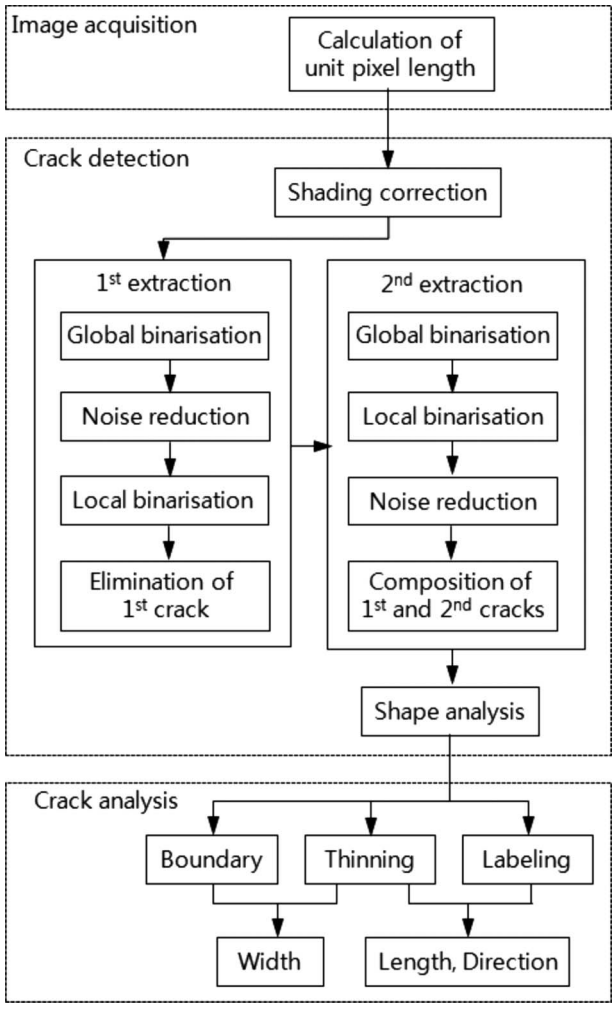

Figure 1. Overview of the proposed algorithm.

camera contains 256 grey scale values. First, the non-uniform brightness in the image is corrected. Then, binarisation based on the thresholding technique and shape analysis is carried out to detect the cracks. The crack characteristics such as crack width, length and orientation are calculated through pre-processing. Lastly, real values of crack characteristics are calculated by multiplying the values of the characteristics obtained in the previous step by the unit pixel length.

2.1. Image acquisition

A digital camera with a CCD size of 23.7 mm × 15.6 mm was used to obtain images of a concrete surface. The optical error is ignored and the lens of camera is assumed to be parallel to the surface. The unit pixel length (α')was defined by dividing the size of the area (ω_{real}) of the obtained image by the number of pixels (N_{pix}). In this study, the unit pixel length was calculated using Equation (1):

$$\alpha' = \frac{\omega_{\text{real}}}{N_{\text{pix}}} = \frac{(l - l_{\text{focus}}) \times \omega_{\text{CCD}}}{l_{\text{focus}} \times N_{\text{pix}}} \times \gamma \qquad (1)$$

where l, l_{focus}, and ω_{ccd} are the distance between the CCD and concrete surface, the focal length, and the width of CCD, respectively. γ is the correction factor according to l and l_{focus}, and is expressed as $0.47(\text{l})^{0.058}$ $(l_{\text{focus}})^{0.075}$. The coefficients of γ were determined using a regression analysis between the left and right sides of Equation (1). For a prime lens camera, is not necessary.

2.2. Crack detection

In the image acquisition step, the amount of light differs with location of concrete surface. Therefore, the background brightness of an image is not uniform if there is no special treatment. To correct this phenomenon, it is essential to normalise the brightness of the background, which makes it possible to improve the detection performance of next step, i.e. binarisation. A morphology technique was adopted to obtain a corrected image (Seul *et al*. 2000). In this study, the subtraction operation followed by openness, which consists of dilation followed by erosion, was applied to correct the non-uniform brightness of the original image, as expressed in Equation (2):

$$C = ((A \oplus B) \ominus B) - A, \qquad (2)$$

where A is the original image and B is the structuring element (in this study, a circle with a 15 pixel radius). $A \oplus B$ is the dilated image of A by the structuring element B. is the eroded image of $A \oplus B$ using the structuring element B. An example of an image before and after correcting the non-uniform brightness is illustrated in Figure 2. The pixel value profile obtained from the corrected image exhibits significantly more uniform background brightness than the original image (Figure 2c and d). From this test, it is exhibited that the morphology-based normalisation successfully processes the correction of non-uniform background brightness.

A method based on the binarisation, which is based on thresholding technique, and shape analysis was developed to distinguish cracks from the background and other defects, as illustrated in Figure 1. All pixels are assigned a value of 1 or 0 and these values represent an object that is based on a set threshold value in a binary image. Therefore, the threshold value is the most important in the detection process. In this study, the Otsu's method was adopted from a series of tests

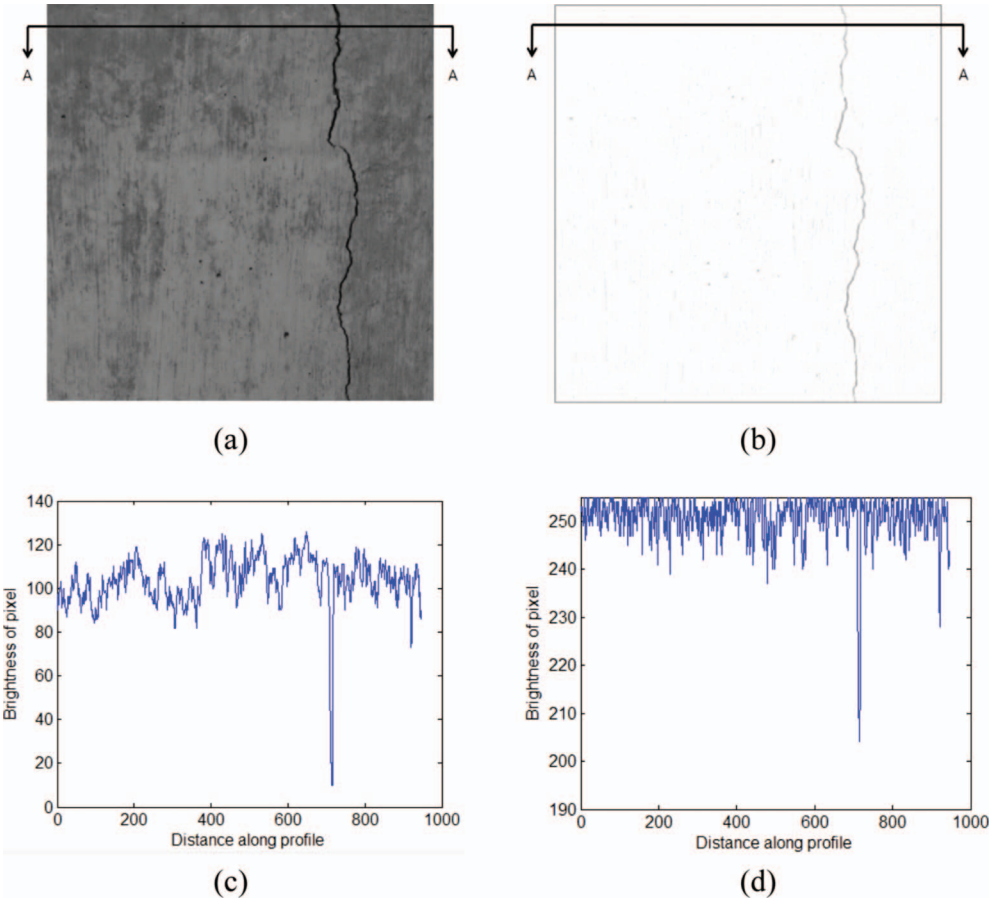

Figure 2. Comparison of images before and after correcting the non-uniformity of brightness for (a) the original image; (b) the corrected image; (c) the pixel value profile obtained from the original image; and (d) the pixel value profile obtained from the corrected image.

(Otsu 1979). To improve the detection performance, a series of additional processes was added to the original simple detection process. It includes noise reduction, local binarisation and a double extraction process. This improvement allows a more accurate crack image to be obtained. If five or more pixels in three-by-three neighbourhood of a pixel have a value of 1, it is set to 1 by the noise reduction process; otherwise, 0 is set to the pixel, which enables to eliminate noise in the image.

Figure 3a shows the object extraction, which follows the above operations in succession. However, only an accurate discrimination between a real object and an extracted object is possible, because global binarisation is performed on the entire image. The next step is local binarisation, which is performed in small areas near the object boundaries extracted in the global binarisation process. The size of each area was optimised to 11 by 11 pixels, and there were five iterations. Figure 3 shows an example of the local binarisation. The results indicate that better object extraction is realised with local binarisation following global binarisation (Figure 3b) than with global binarisation only (Figure 3a).

In order to detect cracks undetected in the first extraction process, a second extraction process was applied. The pixel values of these kinds of cracks are close to those of the background; they are located out of the local binarisation area, as local binarisation is performed according to the object boundaries already detected by the global binarisation. Otsu's method is also adopted for the second process. It uses, however, a modified image in which the objects extracted during the first process have been deleted.

Although the non-uniform brightness is corrected and a series of binarisation processes is performed, there are still some cracks which cannot be distinguishable from other kinds of defects or objects. Therefore, a modified shape factor was considered as a secondary criterion to discriminate the cracks. In this study, a packing density index, which is defined as the division of an object's area by that of the object's circumscribed circle, was adopted (Ammouche *et al*. 2001). As shown

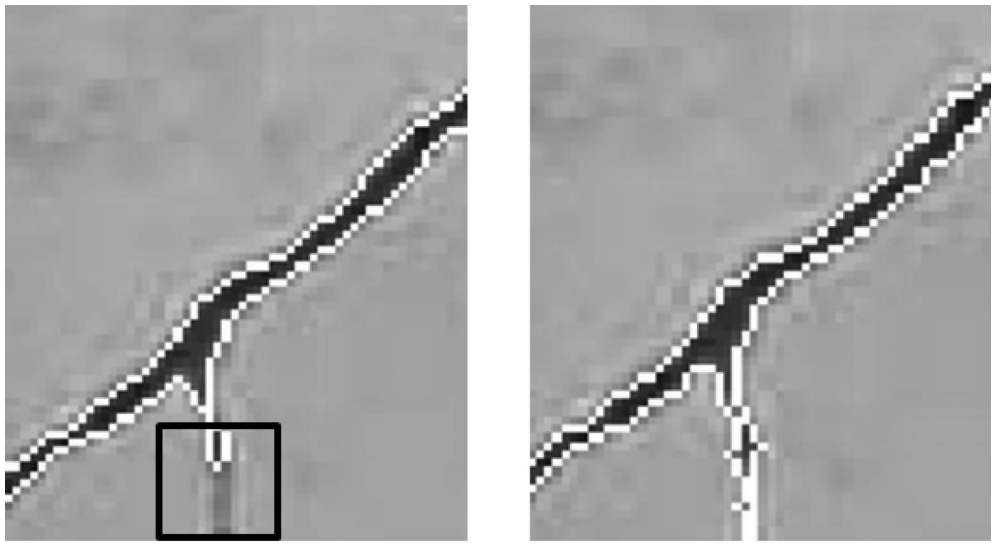

Figure 3. Example of local binarisation for (a) the local area selected for the application of the local binarisation and (b) the result obtained with local binarisation after global binarisation, exhibiting enhanced performance in extracting objects.

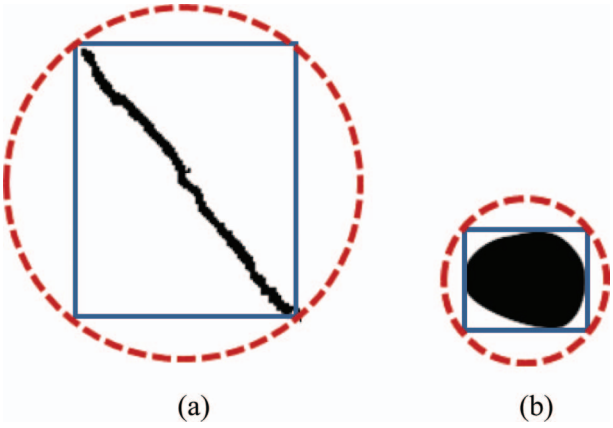

Figure 4. Circumscribed circle of the rectangle that circumscribes (a) a crack-shaped object and (b) a non-crack shaped object.

in Figure 4, this value can then be modified using the circumscribed circle of the rectangle that circumscribes the object rather than the circumscribed circle of the object itself. Through this modification, efficient calculation of the area of the circumscribed circle can be realised. The modified packing density (F_{pd}) is expressed as follows in Equation (3):

$$F_{\mathrm{pd}} = \frac{A_o}{A_{\mathrm{cc}}}, \tag{3}$$

where A_o is the area of the object and A_{cc} is the area of the circumscribed circle of the rectangle that circumscribes the object. F_{pd} tends towards 0 for an extremely elongated object, such as that shown in Figure 4a, or tends towards 1 for a circular object (Figure 4b). After extensive numerical tests, the threshold for distinguishing cracks from other objects, F_{pd}, was empirically optimised to be 0.12.

3. Crack analysis

A series of pre-processing steps was performed to obtain the thinned, boundary and labelled (Haralick and Linda 1992) images shown in Figure 5, which are required to calculate the characteristics of the detected cracks. In this study, the thinning algorithm developed by Zhang was adopted (Zhang and Suen 1984). An object is thinned to a centre line by removing the exterior pixels in a stepwise manner. As a result, an object without holes shrinks to a minimally connected stroke (Figure 5b). The boundary process removes the interior pixels and sets a pixel to 1 if all of its four connected neighbours are 0, thus leaving only the boundary pixels (Figure 5c). A label to an eight-connected object is assigned by the labelling process, which is illustrated in Figure 5d. In the example, three labels were assigned.

The procedure used to determine the crack width is shown in Figure 6a. After carrying out a series of pre-processing steps, the thinned and boundary images of the cracks are incorporated, as shown in Figure 6b. As seen in Figure 6b, the crack width is calculated through the summation of the minimum

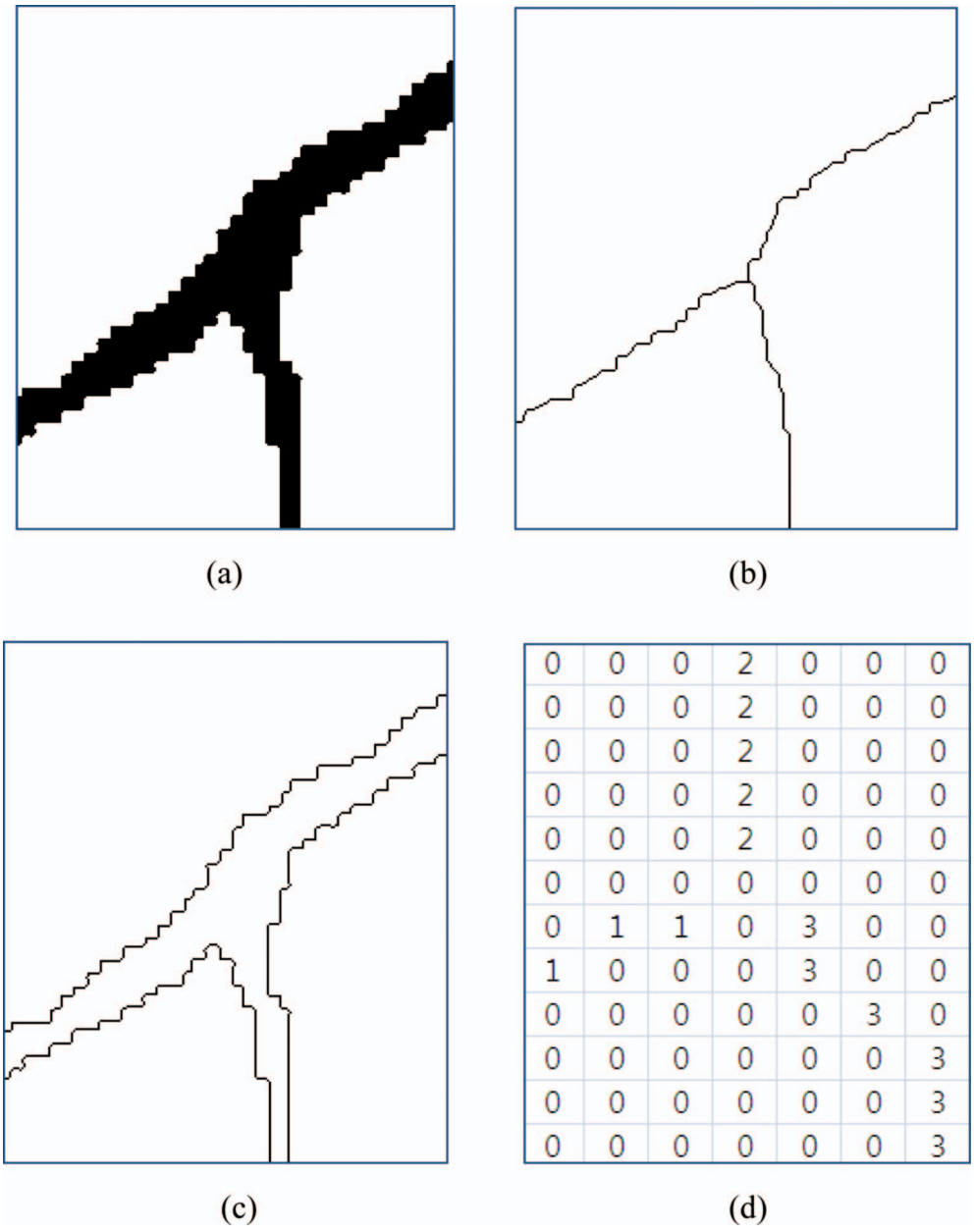

Figure 5. (a) The original image, (b) the thinned image, (c) the boundary image and (d) the labelled image.

distances from the centre pixel to two closest boundary pixels. The four minimum distances from each distance filter were then obtained. From these four values, two minimum distances were selected on the basis of the orientation of the crack. That is to say, if the orientation of cracks is in the range 0–90° and 180–270°, then the filters of A and D are chosen; otherwise, the filters of B and C are chosen. The crack orientation was determined by the positions of two adjacent pixels. In the example shown in Figure 6, the values of filters A and D were chosen because the average orientation of two adjacent pixels is 67.5°. Finally, the real values were calculated by multiplying the crack width calculated based on the pixel coordinate by the unit pixel length.

The algorithm to calculate the crack length and orientation is illustrated in Figure 7. After carrying out pre-processing, the crack was reduced to centre line and each crack has one's unique label, as in the labelled image of Figure 5d. The crack length was calculated

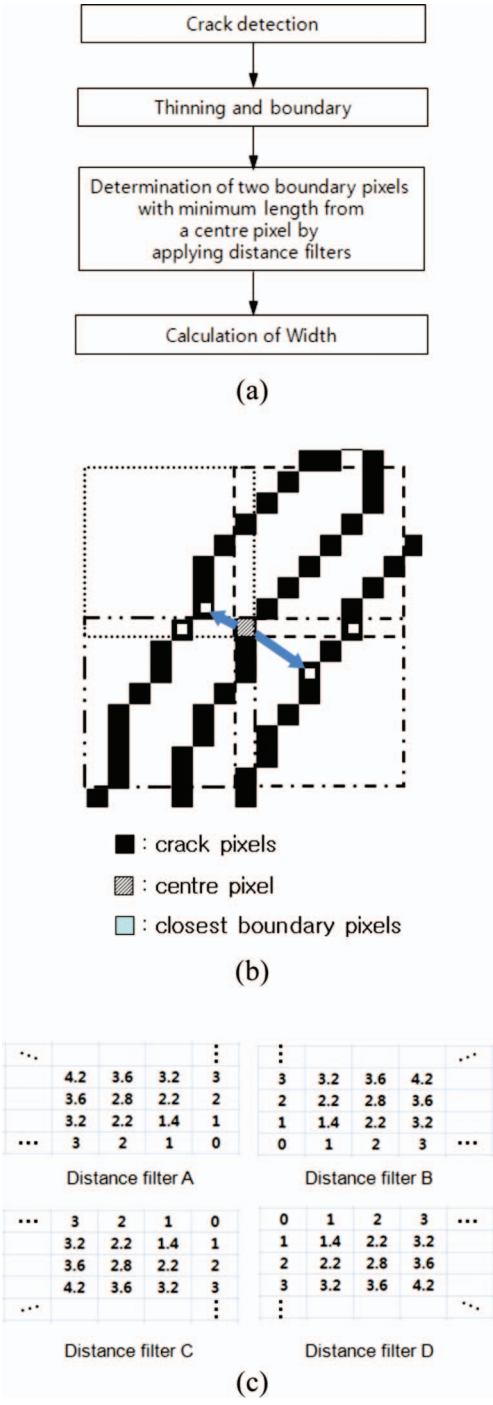

Figure 6. (a) The proposed method for calculating crack; (b) diagram for determining the crack width and (c) the distance filter.

through iteration based on this labelled image. First, the starting pixel was determined. The condition of starting pixel can be expressed by Equation (4):

$$\sum p(i \pm a, j \pm b) = 2 \times l, \tag{4}$$

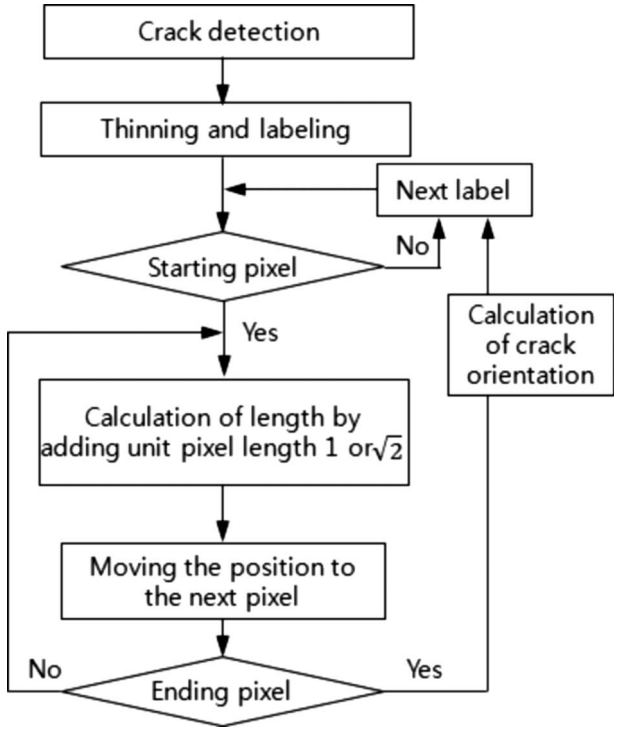

Figure 7. The proposed method for calculating crack length and orientation.

where p is each label number, i and j means the coordinate of each pixels, a and b are both of 0 and 1, and l is a label number. That is to say, the pixel with the sum of values of its nine neighbours being equal to double that of the label number was determined as the starting pixel (Figure 7). Then, depending on the location of the next pixel, the unit pixel length was multiplied by 1.0 or $\sqrt{2}$, and this value was added to the previous value. In the first step, the initial value was zero. The iterative process continues until the ending point is detected. The orientation of the crack, which is calculated using the coordinate relation between the starting pixel and the ending pixel, is expressed in Equation (5) as follows:

$$\angle(i) = \frac{180}{\pi} \times \tan^{-1}\left(\frac{y'(i) - y(i)}{x'(i) - x(i)}\right), \tag{5}$$

where $x(i)$ and $y(i)$ are the coordinates of the starting pixel of the i^{th} crack, and $x'(i)$ and $y'(i)$ are the coordinates of the ending pixel of the i^{th} crack.

To recognise the crack pattern, an artificial neural network is developed. First, the feature was extracted from the image, which is used as input values in the artificial neural network. To extract features, total projection technique is adopted in this study. A feature is the projected length, which is normalised by the maximum projected length to a range between 0 and 1,

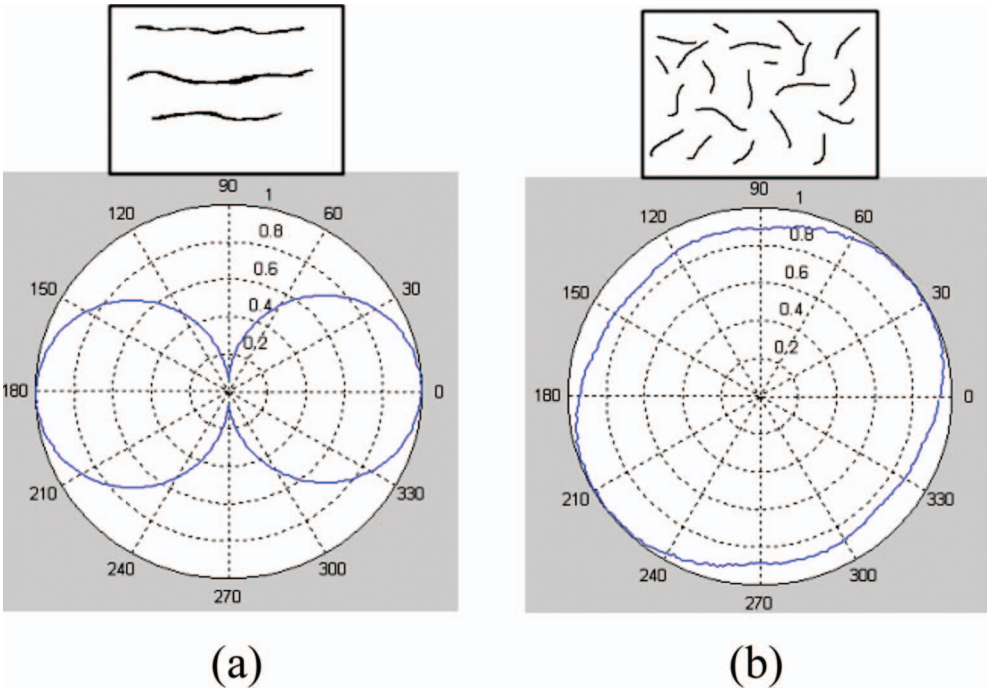

Figure 8. Features for (a) horizontal and (b) random cracks.

Table 1. Target values of output nodes in neural networks for learning.

	Horizontal	Vertical	Diagonal (−45°)	Diagonal (+45°)	Random
node 1	1	0	0	0	0
node 2	0	1	0	0	0
node 3	0	0	1	0	0
node 4	0	0	0	1	0
node 5	0	0	0	0	1

of cracks according to the rotation. Figure 8 shows the typical features for horizontal and random crack. Finally, 60 features for each crack image are determined by averaging 180 projected lengths with 3 values. These features are used as inputs of classifier which is the artificial neural network. The structure of network constructed in this study is 60–4–5 (number of neurons in input layer, 60; number of neurons in hidden layer, 4; and number of neurons in output layer, 5). Moody and Yarvin (1992) have compared the performance of several transfer functions and concluded that the sigmoidal transfer functions performed better than other functions, particularly when the data were noisy and contained non-linear relationships. Therefore, the hyperbolic tangent sigmoid function is used as a transfer function on each neuron. Table 1 represents the target values of output nodes for learning. Weights and biases are determined automatically by the training process. The bayesian regularisation (Mackay 1992, Foresee and Hagan 1997) is adopted as a learning algorithm in order to prevent over-fitting. The output node with maximum output value represents the relevant crack pattern. Figure 9 shows the developed crack detection and analysis program.

4. Validation of the method

To assess the validity of the proposed technique, a series of tests was performed on real crack images taken with a digital camera. Figure 10 shows four types of crack images and the resulting detected images: Figure 10a shows numerous meaningless objects and cracks; Figure 10b shows a branch-shaped crack; Figure 10c shows several small cracks along a main crack; and Figure 10d shows a crack, stains and small holes. Figure 10a shows that the cracks are clearly distinguishable from small holes, and the branch-shaped crack in Figure 10b is also very distinct. Figure 10c shows satisfactory performance using the proposed algorithm, as several narrow and randomly short cracks along the main crack are indicated. The second extraction process made it possible to detect these cracks. On the other hand, the small crack along the main crack in Figure 10c was not clearly detected because the crack's modified packing density, F_{pd}, was greater than the threshold value of 0.12. While this crack could have been detected by employing an increased the threshold value of F_{pd}, such an increase

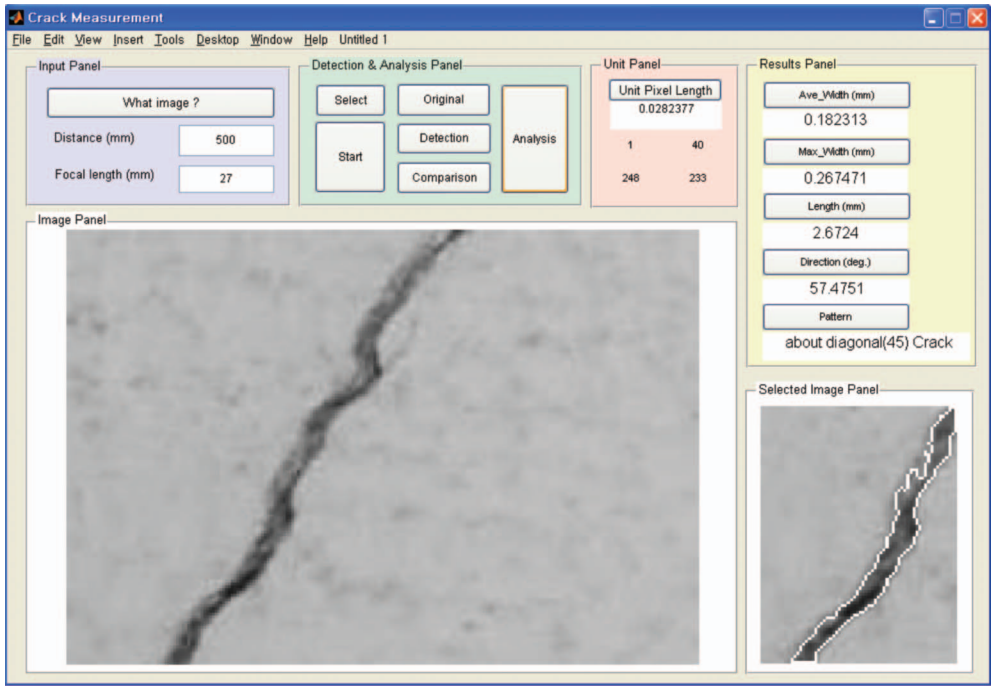

Figure 9. Software for crack detection and analysis.

might have led to a greater incidence of meaningless objects or noise being falsely detected as cracks. Figure 10d shows that the crack is clearly distinguishable from noise, such as the stains and small holes that represent a concrete surface similar to that exposed to the environment for an extended period of time. Through a comparison of the original crack images with the results obtained using the proposed technique, the validity of the proposed technique is confirmed by the accurately detected crack images.

The effect of focal lengths and distances between the camera and concrete surface on the measurement accuracy was investigated to verify the performance of the developed technique under the conditions at the image acquisition. The test results obtained for five measurement points are listed in Table 2. The standard deviation of the crack width calculated under the test conditions was 0.024–0.045 and their average was 0.036. This deviation is mainly attributed to the difference in the image resolution. The accuracy of a measuring technique using image processing depends on the resolution, which depends on the specification of device and distance between device and concrete surface at image acquisition step. Although this phenomenon was observed in these tests, it can be ignored in the test conditions. The crack widths calculated by the proposed technique and the values measured by an optical crack microscope are listed in Table 3. The results showed very similar numerical values. The relative difference (RD) between the two values were defined by the following Equation (6) and are in the range of 0.67–5.9% (average: 3.8%):

$$\mathrm{RD} = \frac{|w_{\mathrm{new}} \times w_{\mathrm{con}}|}{w_{\mathrm{con}}}, \tag{6}$$

where w_{new} is the crack width calculated using the proposed technique and w_{con} is the crack width measured using the optical crack microscope. Although there are some errors, the present results suggest that the proposed technique can provide sufficient accuracy to measure the crack width in practical contexts.

Tables 4 and 5 compare the crack lengths (l_{new}) and crack orientations (o_{new}) calculated using the proposed technique, and the length values (l_{con}) measured by a ruler (resolution: 1 mm) and orientation values (o_{con}) measured by a protractor (resolution: 1°), respectively. The RD between the two values was also defined using Equation (6). A large error was observed in the measured crack length, which is attributed to the use of a straight ruler. If the crack length was measured by dividing it into several segments, the accuracy will be increased.

Table 6 shows the results of pattern recognition of cracks by the artificial neural network. It is exhibited that the classifier constructed in this study can effectively classify cracks into five categories.

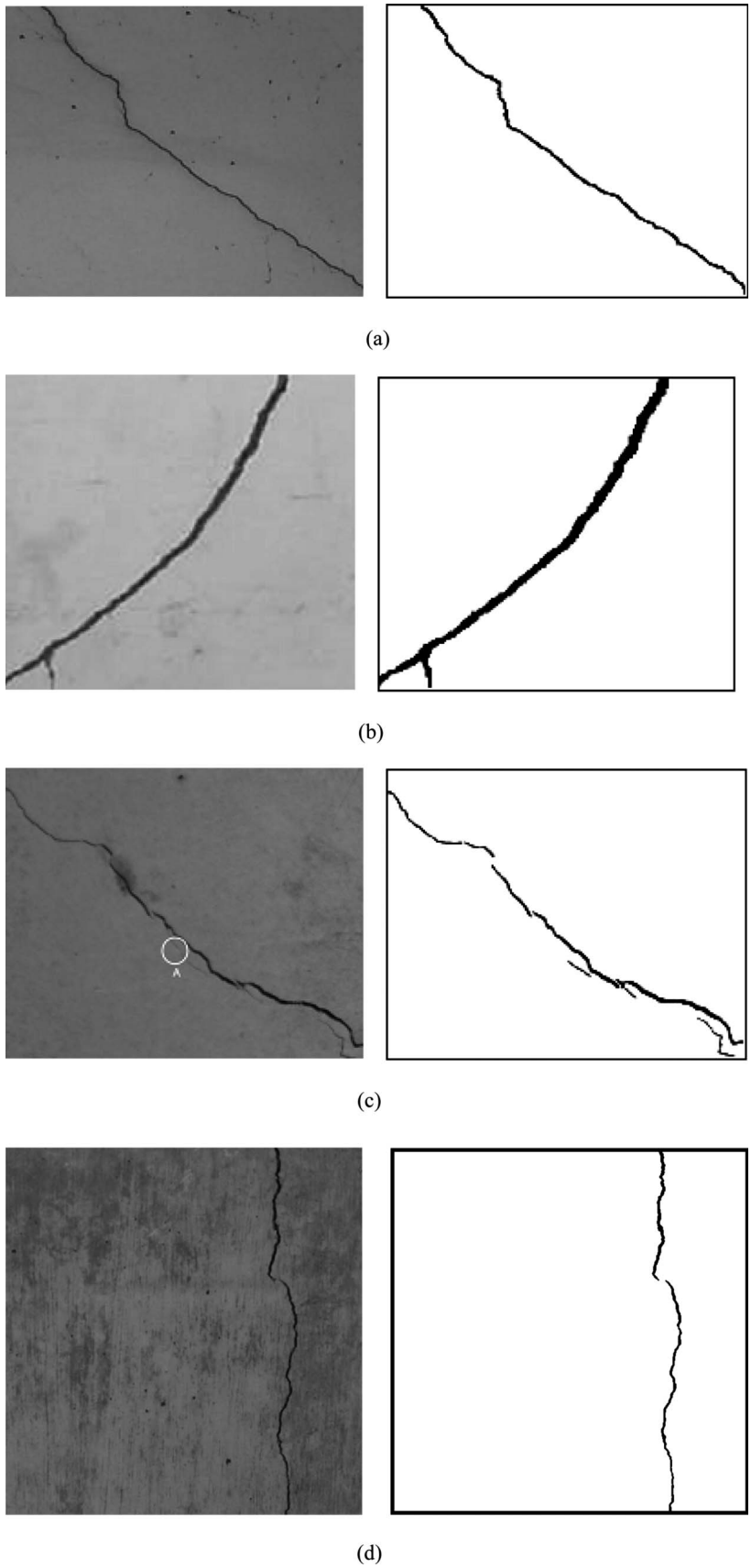

Figure 10. Results of crack detection.

Table 2. Crack width measured under the condition of several focal lengths of camera and distances between camera and concrete surface.

Distance between camera and cracks (mm)	Focal length (mm)	Unit pixel length (mm/pixel)	No.				
			1	2	3	4	5
865	28	0.209	1.05	1.49	0.89	–	–
865	50	0.119	–	1.48	0.84	0.84	–
1200	28	0.299	1.02	1.57	0.90	0.90	1.02
1200	50	0.171	–	1.55	0.83	0.86	1.07
1200	70	0.124	–	1.48	0.82	0.87	
1915	50	0.286	1.10	1.50	0.86	0.86	0.98
1915	70	0.207	–	–	0.83	0.83	–
Average (mm)			1.05	1.51	0.85	0.86	1.02
Standard deviation (mm)			0.040	0.039	0.031	0.024	0.045

Table 3. Results of crack width measurement.

	No.				
	1	2	3	4	5
w_{new} (mm)	1.05	1.51	0.85	0.86	1.02
w_{con} (mm)	1.0	1.5	0.8	0.9	1.0
RD (%)	5.5	0.67	5.9	4.7	2.3

Table 4. Results of crack length measurement.

	No.				
	1	2	4	5	6
l_{new} (mm)	680.6	312.3	561.5	112.6	121.3
l_{con} (mm)	630	300	540	100	100
RD (%)	8.03	4.10	3.98	12.6	21.3

Table 5. Results of crack orientation measurement.

	No.				
	1	2	4	5	7
o_{new} (mm)	−71.6	−74.4	−63.4	−61.7	65.6
o_{con} (mm)	−70	−75	−65	−60	66
RD (%)	2.2	0.85	2.4	2.8	0.67

Table 6. Results of pattern recognition of cracks by artificial neural network.

Classifications by human	Classifications by artificial neural network						
	Horizontal	Vertical	−45°	+45°	Random	Total	Accuracy (%)
Horizontal	4	0	0	0	0	4	100
Vertical	0	19	0	0	0	19	100
Diagonal (−45°)	0	0	7	0	0	7	100
Diagonal (+45°)	0	0	0	5	0	5	100
Random	0	0	0	0	3	3	100

5. Summary and conclusions

This paper proposed an image processing technique for the automatic detection and analysis of cracks in the digital image of a concrete surface. A series of experimental and analytical investigations were performed to assess the validity of this technique. The following conclusions have been drawn from the current results.

(1) A morphological technique was applied to correct the non-uniformity of the background brightness of the images. Through comparisons with the pixel value profiles of the original image and the corrected image, it is exhibited that the morphology-based normalisation successfully processes the correction of non-uniform background brightness.
(2) A local binarisation process, double extraction processes and additional criteria based on shape analysis were proposed to enhance the detection performance of cracks. Then tests were carried out to test the detection

performance of proposed method. Test results showed that the proposed detection algorithm can provide accurate crack detection on several types of crack images such as the crack image including meaningless objects, branch-shaped crack, several small cracks along a main crack and crack image with textile background and stains.

(3) Specific algorithms for calculating the crack width, length and orientation, and crack pattern recognition technique based on an artificial neural network were proposed. Then a series of experimental tests was carried out to verify the feasibility to the analysis of cracks and accuracy of proposed methods. It cannot be concluded that test results reflect the accuracy of the proposed technique simply due to the errors in the measured data. However, at a minimum, the present results suggest that the proposed technique can provide sufficient accuracy for analysing the characteristics of surface cracks in practical contexts.

Acknowledgements

This work was supported by a grant from the Korean Ministry of Education, Science and Technology (The Regional Core Research Program/Biohousing Research Institute) and was also supported by the Biohousing Research Centre.

References

Ammouche, A., *et al*., 2001. A new image analysis technique for the quantitative assessment of microcracks in cement-based materials. *Cement and Concrete Research*, 30 (1), 25–35.

Chen, L.C., *et al*., 2006. Measuring system for cracks in concrete using multitemporal images. *Journal of Surveying Engineering*, 132 (2), 77–82.

Foresee, F.D. and Hagan, M.T., 1997. Gauss-Newton approximation to Bayesian learning. *In*: *Proceedings of the 1997 international joint conference on neural networks*. Piscataway: IEEE, 1930–1935.

Haralick, R.M. and Linda, G.S., 1992. *Computer and robot vision*. Volume I. New York: Addison-Wesley, 28–48.

Hutchinson, T.C. and Chen, Z., 2006. Improved image analysis for evaluating concrete damage. *Journal of Computing in Civil Engineering*, 20 (3), 210–216.

Ito, A., Aoki, Y., and Hashimoto, S., 2002. Accurate extraction and measurement of fine cracks from concrete block surface image. *IEEE Industrial Electronics Society*, 3, 2202–2207.

Kaseko, M.S. and Ritchie, S.G., 1993. A neural network based methodology for pavement crack detection and classification. *Transportation Research. Part C, Emerging Technologies*, 1 (4), 275–291.

Mackay, D.J.C., 1992. Bayesian interpolation. *Neural Computation*, 4 (3), 415–447.

Moody, J.E. and Yarvin, N., 1992. Networks with learned unit response functions. *In*: J.E. Moody, S.J. Hanson, and R.P. Lippmann, eds. *Advances in neural information processing systems 4*. San Mateo: Morgan Kaufmann Publishers, 1048–1055.

Oh, J.K., *et al*., 2009. Bridge inspection robot system with machine vision. *Automation in Construction*, 18, 929–941.

Otsu, N.A., 1979. Threshold selection method from gray level histogram. *IEEE Transactions on Systems*, SMC-9 (1), 62–66.

Schutter, G.D., 2002. Advanced monitoring of cracked structures using video microscope and automated image analysis. *NDT & E International*, 35 (4), 209–212.

Seul, M., O'Gorman, L., and Sammon, M.J., 2000. *Practical algorithms for image analysis*. New York: Cambridge University Press.

Sinha, S.K. and Fieguth, P.W., 2006. Automated detection of cracks in buried concrete pipe images. *Automation in Construction*, 15, 58–72.

Sohn, H.G., *et al*., 2005. Monitoring crack changes in concrete structures. *Computer-Aided Civil and Infrastructure Engineering*, 20, 52–61.

Yamaguchi, T., *et al*., 2008. Image-based crack detection for real concrete surfaces. *Transactions on Electrical and Electronic Engineering*, 3, 128–135.

Yu, S.N., Jang, J.H., and Han, C.S., 2007. Auto inspection system using a mobile robot for detecting concrete cracks in a tunnel. *Automation in Construction*, 16, 255–261.

Zhang, T.Y. and Suen, C.Y., 1984. A fast parallel algorithm for thinning digital patterns. *Communications of the ACM*, 27 (3), 236–239.